PERGAMON

Chemosphere 53 (2003) 715–725

CHEMOSPHERE

www.elsevier.com/locate/chemosphere

Laboratory evaluation of zero-valent iron to treat water impacted by acid mine drainage

Richard T. Wilkin *, Mary S. McNeil

Office of Research and Development, National Risk Management Research Laboratory, US Environmental Protection Agency, Robert S. Kerr Environmental Research Lab, 919 Kerr Research Drive, Ada, OK 74820, USA

Received 30 October 2002; received in revised form 10 April 2003; accepted 14 April 2003

Abstract

This study examines the applicability and limitations of granular zero-valent iron for the treatment of water impacted by mine wastes. Rates of acid-neutralization and of metal (Cu, Cd, Ni, Zn, Hg, Al, and Mn) and metalloid (As) uptake were determined in batch systems using simulated mine drainage (initial pH 2.3–4.5; total dissolved solids 14 000–16 000 $mg\,l^{-1}$). Metal removal from solution and acid-neutralization occurred simultaneously and were most rapid during the initial 24 h of reaction. Reaction half-lives ranged from 1.50 ± 0.09 h for Al to 8.15 ± 0.36 h for Zn. Geochemical model results indicate that metal removal is most effective in solutions that are highly undersaturated with respect to pure-metal hydroxides suggesting that adsorption is the initial and most rapid metal uptake mechanism. Continued adsorption onto or co-precipitation with iron corrosion products are secondary metal uptake processes. Sulfate green rust was identified as the primary iron corrosion product, which is shown to be the result of elevated $[SO_4^{2-}]/[HCO_3^-]$ ratios in solution. Reversibility studies indicate that zero-valent iron will retain metals after shifts in redox states are imposed, but that remobilization of metals may occur after the acid-neutralization capacity of the material is exhausted.

Keywords: Zero-valent iron; Groundwater remediation; Permeable reactive barrier; Acid mine drainage

1. Introduction

Acid mine drainage (AMD) is an environmental problem that causes adverse effects to the quality groundwater and surface water. It is principally caused by the oxidation of metal sulfide minerals contained in mine wastes, especially the iron disulfide pyrite (Lowson, 1982; Williamson and Rimstidt, 1994). About 19 300 km of rivers and streams and more than 180 000 acres of lakes and reservoirs in the continental US have been damaged by AMD (Kleinmann, 1989). Studies conducted by the California Department of Fish and Game have shown as many as 47 000 fish killed at one site during a 7-day period in 1967 as a direct consequence of AMD (Nordstrom et al., 1977). Surface waters impacted by AMD can be identified by low pH, typically between pH 2 and 4, elevated concentrations of iron, sulfate, total dissolved solids (TDSs), and heavy metals, most of which are toxic to living organisms. Compared to the low pH and oxidizing nature of affected surface water, groundwater impacted by AMD typically is less acidic and more reducing due buffering reactions with hydroxide, carbonate and aluminosilicate minerals present in aquifers (e.g., Blowes and Ptacek, 1994) and due to the consumption of dissolved oxygen and exclusion of air in subsurface environments (e.g., Barnes and Clarke, 1964).

* Corresponding author. Tel.: +1-580-436-8874; fax: +1-580-436-8703.

E-mail address: wilkin.rick@epa.gov (R.T. Wilkin).

0045-6535/$ - see front matter © 2003 Elsevier Ltd. All rights reserved.
doi:10.1016/S0045-6535(03)00512-5

Although the effects of AMD are most evident in surface waters, infiltration through crushed mill tailings and waste rock piles can degrade the quality of groundwater resources around active and inactive mine sites and consequently there is a need to develop cost-effective approaches for remediating groundwater impacted by mine wastes. The use of subsurface permeable reactive barriers (PRBs) presents a passive approach for removing metals from groundwater (Blowes et al., 2000). A major challenge facing the development of the PRB technology for groundwater remediation is the selection and evaluation of reactive media that can be employed to provide a long-term sink for metals while at the same time maintain permeability and hydraulic connectivity between the contaminant plume and the reactive treatment zone.

Compost-based reactive media for subsurface systems (e.g., leaf mulch, sawdust, sewage sludge, wood chips) have been extensively studied by Waybrant et al. (1998, 2002). This treatment strategy is analogous to the use of anaerobic solid-substrate bioreactors for removing metals from solution (e.g., Dvorak et al., 1992; Drury, 1999; Steed et al., 2000). Compost-based treatment relies on bacterially mediated sulfate-reduction to increase alkalinity, remove sulfate, and remove metals through the formation of insoluble sulfide precipitates (Benner et al., 1997, 1999).

Zero-valent iron has also been shown to successfully treat acidic water contaminated with heavy metals such as chromium, uranium, arsenic, manganese, and zinc (e.g., Cantrell et al., 1995; Shelp et al., 1995; Puls et al., 1999; Shokes and Möller, 1999; Lackovic et al., 2000; Morrison et al., 2002). In most cases, metal removal mechanisms are not well understood but are believed to involve both adsorption and reductive mineral precipitation processes. In this study, we evaluate acid-neutralization rates and removal rates of Fe, Al, Cu, Zn, Cd, As(V), Hg, Mn, and Ni using zero-valent iron in batch studies. The nature of secondary solids formed during water treatment with zero-valent iron is examined to understand the mechanisms involved in metal removal and implications regarding the long-term stability of metals sequestered in the reactive media.

2. Materials and methods

2.1. Synthetic AMD solution and reactive media

Bench-top studies were conducted using Peerless iron (Peerless Metal Powders and Abrasive, Inc.), Fisher iron, and synthetic AMD solutions with initial pH of 2.3, 3.5, and 4.5. Solutions were prepared by adding aliquots of concentrated ultra-pure sulfuric acid to a 0.10 M Na_2SO_4 solution. Metal stock solutions were prepared from reagent grade salts and then added to the 0.10 M Na_2SO_4 solution to bring concentrations to approximately 10 mg l^{-1} As(V), 5 mg l^{-1} Ni, 5 mg l^{-1} Cd, 65 mg l^{-1} Cu(II), 3 mg l^{-1} Hg(II), 20 mg l^{-1} Mn(IV), and 65 mg l^{-1} Zn. Ferric chloride (3 mM) was added to the pH 2.3 solution and aluminum sulfate was added to the pH 2.3 and the pH 3.5 experiments (5 and 0.05 mM, respectively). The iron and aluminum concentrations were selected to be undersaturated with respect to amorphous $Fe(OH)_3$ and $Al(OH)_3$. Table 1 shows the initial metals concentrations in each batch series.

Two types of zero-valent iron were evaluated in the batch studies, Peerless iron (−8 + 50 mesh particle size, WSR) and Fisher iron (−100 mesh particle size). The mass concentration of Fe^0 (ρ_m) ranged from 0.02 to 0.23 g ml^{-1}. Specific surface areas were determined for each iron type using a Coulter SA 3100 Surface Area Analyzer; the Peerless iron had a pre-exposure specific surface area of 3.05 $m^2 g^{-1}$ and the Fisher iron had a pre-exposure specific surface area of 0.05 $m^2 g^{-1}$.

Table 1
Initial and final solute concentrations and pH

Batch experiment	SO_4^{2-} (mg l^{-1})	Fe (mg l^{-1})	Al (mg l^{-1})	Hg (mg l^{-1})	As (mg l^{-1})	Cd (mg l^{-1})	Cu (mg l^{-1})	Mn (mg l^{-1})	Ni (mg l^{-1})	Zn (mg l^{-1})	pH
Initial pH 2.3	11 300	154	126	3.1	10.4	5.0	61	18	4.6	60	2.3
10 g Peerless[a]	8870	671	0.12	<0.07	0.06	0.08	<0.01	54	<0.01	0.71	5.7
10 g Peerless	9060	142	0.07	<0.07	<0.01	0.02	<0.01	36	<0.01	0.39	6.0
10 g Fisher[a]	5410	287	0.03	<0.07	<0.01	0.04	<0.01	13	<0.01	0.13	5.3
1 g Peerless[a]	10 300	974	0.03	<0.07	<0.01	0.69	<0.01	25	0.01	13	5.5
initial pH 3.5	9950	<0.1	1.3	3.1	9.8	4.9	61	17	4.4	64	3.5
10 g Peerless[b]	9600	<0.1	0.03	<0.07	0.04	<0.01	0.03	0.04	<0.01	0.04	9.4
10 g Peerless	9580	<0.1	0.04	<0.07	0.05	<0.01	<0.01	0.01	<0.01	0.02	10.0
1 g Peerless[b]	9720	88	0.04	<0.07	<0.01	1.67	1.83	19	0.32	17	5.7
initial pH 4.5	9730	<0.1	0.1	2.1	10.2	5.3	61	18	4.8	66	4.5
10 g Peerless	9240	0.12	0.05	<0.07	0.05	<0.01	<0.01	0.03	<0.01	<0.01	9.8

[a] Initial solution 5 mM Al(III) and 3 mM Fe(III).
[b] Initial solution 0.05 mM Al(III); final concentrations correspond to 450 h of reaction.

2.2. Experimental set-up and analyses

Iron metal was first added to a series 44 ml glass vials followed by the synthetic AMD solution allowing for zero headspace. Water volumes were determined gravimetrically. The glass vials were capped with Teflon-lined septa. Each vial was placed on an orbital shaker at 108 rpm until sampling. A separate vial was retrieved and sampled at time intervals ranging from 0 to 450 h. Control samples containing no iron filings were collected and analyzed at time intervals of 0, 75, and 350 h. In all cases control samples showed stable pH values and no loss of initial metal concentrations. Batch reactions were carried out at ambient temperature (22 ± 1 °C). Samples were collected for the analysis of metals, sulfate, arsenic speciation, total Fe, pH, oxidation–reduction potential (ORP), and temperature.

A disposable syringe was used to withdraw approximately 15 ml aliquots for metals analyses. The solution aliquot was filtered through a 0.22 μm membrane filter (mixed cellulose ester) and preserved with ultrapure nitric acid (pH < 2.0). Metals concentrations were determined using inductively coupled plasma-optical emission spectroscopy (ICP-OES; Perkin Elmer Optima 3300 DV). For some samples, concentrations of As and Hg were determined by using graphite furnace atomic absorption spectroscopy (GFAAS, Perkin-Elmer 5100PC) because of a need for low detection limits. Next, a sample was collected for sulfate analysis; 1 ml of sample was removed from the reaction vial and diluted with approximately 9 ml of deionized water. Sulfate concentrations were determined using capillary electrophoresis (Waters Quanta 4000E). All samples were stored at 4 °C until quantitative analysis was complete. Analyses of duplicate and spiked samples indicated an analytical error of less than 3% for all parameters analyzed in the laboratory.

Samples for arsenic speciation were filtered through a 0.22 μm syringe filter, preserved with ultrapure hydrochloric acid (pH < 2.0), and analyzed by ion chromatograph–hydride generation–atomic fluorescence spectrometer (IC–HG–AFS; IC, DIONEX, and HG–AFS, PSA Excalibur). Arsenite and arsenate were first separated by an ion chromatograph, then reacted to form arsine through a hydride generation apparatus, and finally detected by an atomic fluorescence spectrometer. The system was able to quantify arsenic to 5 $\mu g\,l^{-1}$ in undiluted samples.

A sample aliquot was analyzed for total iron using the 1,10-phenanthroline + reductant method (HACH FerroVer) and a HACH DR2010 spectrophotometer. Ferrous iron was determined by using the 1,10-phenanthroline reagent but without the hydrosulfite reductant. Ferric iron was calculated from the difference of total iron and ferrous iron measurements. The remaining solution was removed to measure pH and ORP. Electrode calibration and performance was checked before sample measurement. The pH electrode (Corning Semi-Micro No. 476156) was calibrated using standard NIST-traceable pH 2.0, 4.0, 7.0, and 10.0 buffers, and the ORP electrode (Orion 9678 BN) was checked using the Orion ORP solution (Orion 967961). The measured ORP values were converted to E_h values by adding the difference between the measured ORP of the reference solution and the theoretical ORP of the reference solution.

2.3. Solid-phase characterization

A parallel set of batch experiments were conducted for the purpose of extracting and analyzing the iron corrosion products that precipitated as the iron filings reacted with the various AMD solutions. Glass vials containing the experimental products were transferred to an anaerobic chamber, opened, and the fine-grained precipitates collected by filtration after sonication. A magnet was used to retain the iron filings in the glass vial, while loose precipitates were filtered through a 0.4 μm membrane filter (47 mm). This process was repeated several times after rinsing in order to collect as much of the precipitate mass as possible. The precipitates were allowed to dry inside the glove box under an anoxic N_2–H_2 atmosphere. While still in the glove box, about 10 mg of material was mounted on zero-background quartz plate and mixed with glycerol to retard air oxidation. The quartz plate was removed from the glove box and analyzed with a Rigaku Miniflex X-ray diffractometer at a scan rate of 0.5° 2-theta per minute (Cu Kα radiation; operated at 30 keV and 15 mA). The composition of the corrosion products was determined by ICP-OES after microwave digestion in dilute nitric acid. Total sulfur measurements were made with a UIC sulfur coulometer system. Precipitate samples were covered with V_2O_5 and combusted in the presence of oxygen at 1050 °C. Evolved gases pass through a column of reduced Cu to quantitatively convert all sulfur to SO_2. The gas stream is then carried to the coulometer cell where it is absorbed and coulometrically titrated. Particle morphology and composition was also determined using a JEOL JSM-5300 scanning electron microscope equipped with an Oxford Instruments energy dispersive X-ray spectroscopy (EDX) system. The weight and atomic percentage of the elements present on the iron grains were semi-quantitatively determined using EDX.

3. Results and discussion

3.1. pH and redox

The pH of batch experiments increased from initial values of 2.3–4.5 to final values of 5.5–10.0. In all cases the pH increase was most rapid in the first 24 h of

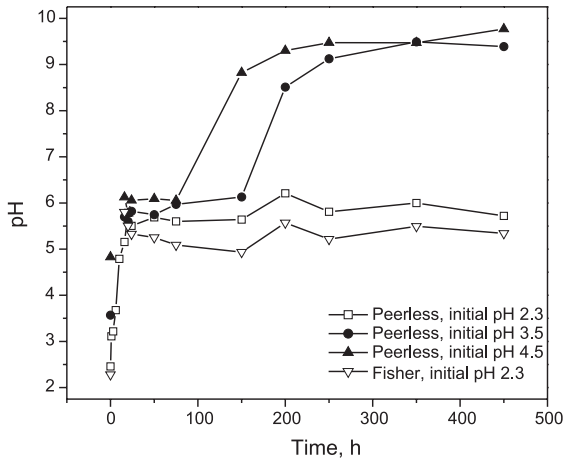

Fig. 1. Time-dependent changes in pH as a function of initial conditions.

reaction. Over this initial reaction period between 1.4 and 225 μmol H^+ l^{-1} were consumed depending on the initial pH. The final pH was controlled primarily by the initial pH and the mass concentration of Fe^0 (Table 1). In the low pH experiments with added Al(III) and Fe(III), lower final pH was attained due to the additional source of acidity provided by hydrolysis of Al(III) and Fe(III). The E_h of the batch systems decreased from a maximum value of about 750 mV (pH 2.3 experiments) to minimum values of 200 to −200 mV. In general trends in E_h were variable, but showed consistent trends from highly oxidizing conditions to moderately reducing conditions.

Time-dependent pH values are plotted in Fig. 1. In the pH 2.3 series, regardless of the mass concentration of Fe^0, the pH increased to approximately pH 5.7–6.0. Higher initial pH conditions resulted in final pH values of 9.6–10.0 after 450 h of reaction (Fig. 1). Fisher iron showed similar trends in pH and metal removal efficiency as compared to Peerless iron (see Table 1).

3.2. Metal concentrations

Time-dependent changes in the concentrations of Fe, Al, Mn, Cu, Zn, Ni, Cd, Hg, and As are shown in Fig. 2. Experiments at an initial pH of 2.3 resulted in significant decreases in metal concentrations, except for iron and manganese (Table 1, Fig. 2a). Manganese concentrations more than doubled with final concentrations up to 54 mg l^{-1}, indicating that dissolution of zero-valent iron resulted in the release of Mn and that the pH increase was not sufficient to drive Mn hydroxide precipitation. Similarly iron concentrations increased from an initial value of approximately 150–670 mg l^{-1}. Initially iron was present as Fe(III) but within the first several hours of reaction, Fe(III) vanished from solution and total iron concentrations were dominated by Fe(II). The loss of nickel, cadmium, arsenic, mercury, copper, and zinc from solution corresponds most directly to the increase in pH caused by the anaerobic dissolution of zero-valent iron:

$$Fe^0 + 2H^+ = Fe^{2+} + H_2$$

Decreases in the initial solid/solution ratio resulted in less effective removal of cadmium and zinc (Table 1). Note that high concentrations of sulfate as employed in these experiments might be expected to enhance the overall iron corrosion process relative to pure water systems (Gui and Devine, 1994).

Arsenic speciation was determined in samples collected from the initial pH 2.3 systems at time intervals from 0 to 24 h. Speciation results indicate that the zero-valent iron did not change the oxidation state of arsenic in solution as As(V) was the only form detected, consistent with previous investigations (e.g., Lackovic et al., 2000; Su and Puls, 2001).

The presence of Al(III) or Fe(III) in the initial solution had little affect on the apparent metal removal efficiency of the zero-valent iron. In initial solutions near-saturated in amorphous $Fe(OH)_3$, and $Al(OH)_3$, concentrations of copper, arsenic, and mercury all decreased to less than analytical detection limits, while concentrations of nickel and cadmium were reduced to less than 0.065 mg l^{-1} after 450 h of reaction. Zinc decreased to as low as 0.2% of initial values.

At initial pH of 3.5 ($\rho_m = 0.23$), concentrations of aluminum, mercury, cadmium, and nickel were reduced to below nominal detection limits and zinc, arsenic, copper, and manganese concentrations were reduced to below 0.04 mg l^{-1} after 450 h of reaction. Concentrations of iron increased over the first 20 h of reaction, reaching 48 mg l^{-1}, before decreasing to final values below 0.1 mg l^{-1}. Metal removal trends were independent of the initial presence or absence of dissolved Al. In systems with initial pH of 3.5 ($\rho_m = 0.02$), manganese concentrations remained at approximately 18.0 mg l^{-1}, rather than increasing as in the batch experiments at initial pH 2.3.

Batch studies at an initial pH of 4.5 were conducted to evaluate the metal uptake by 10 g of Peerless iron (Fig. 2b). Such conditions are perhaps more typical of groundwater contaminated by AMD (Langmuir, 1997). Mercury, cadmium, copper, and nickel concentrations were all reduced to less than detection limits. Arsenic and manganese were reduced to less than 0.05 mg l^{-1}. Total iron increased over the first 75 h of reaction before declining to a final concentration of 0.118 mg l^{-1} after 450 h (Fig. 2b).

3.3. Sulfate concentrations

Sulfate is the dominant anion in mine drainage waters and in the solutions used in this study. Initial sulfate

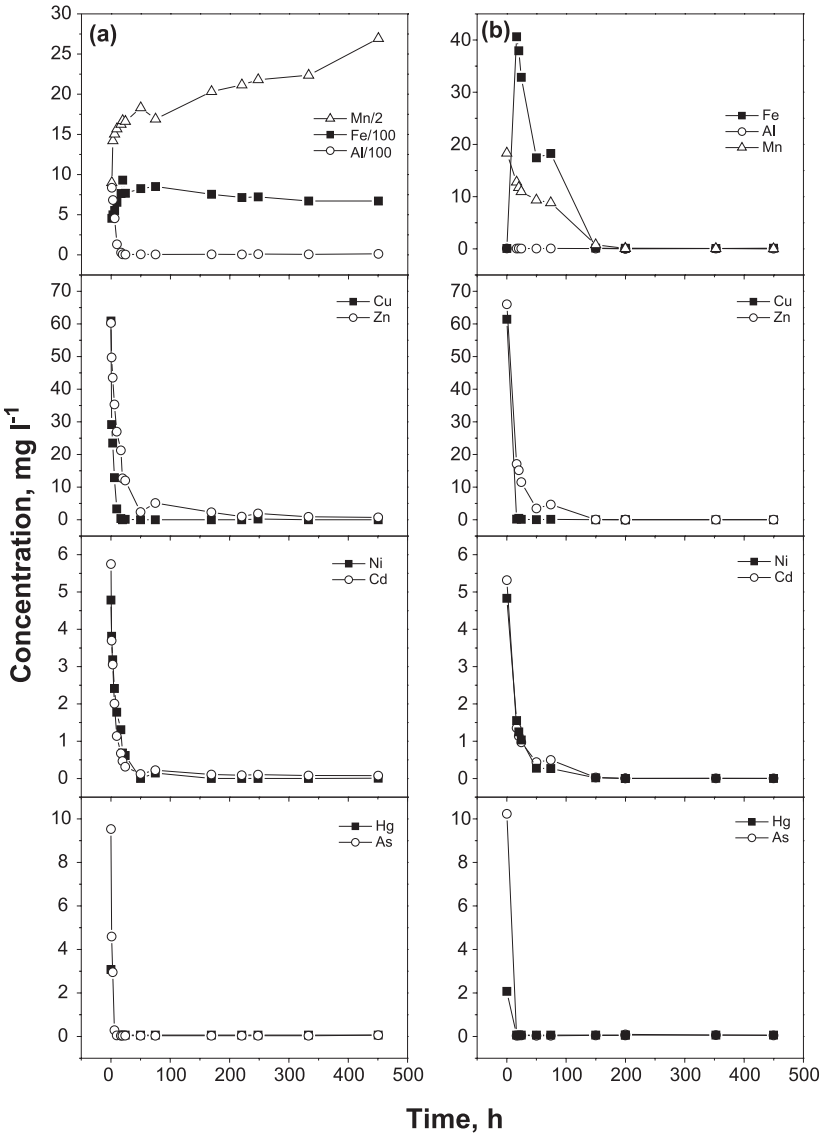

Fig. 2. Changes in metal concentrations with time: (a) initial pH 2.3 and (b) initial pH 4.5.

concentrations in the batch experiments ranged from about 10 000 to 11 000 mg l^{-1}. Final sulfate concentrations were slightly lower (8900–9500 mg l^{-1}) compared to initial values after reaction with Peerless iron, suggesting some removal mechanism for sulfate (see also Shokes and Möller, 1999). Reduction of sulfate concentrations was more evident in experiments with Fisher iron; sulfate concentrations decreased by as much as a factor of 2 when Fisher iron was used (Table 1). The removal of sulfate from solution corresponds to the formation of iron corrosion products as discussed in a following section. The results of these batch studies, however, are in stark contrast to field deployments of zero-valent iron reactive barriers where sulfate is often entirely removed from groundwater plumes. The discrepancy between the field and lab results relates to microbial respiration of sulfate-reducing bacteria, which is common in field deployments (e.g., Phillips et al., 2000) but absent in most bench-top studies.

3.4. Metal removal rates

The rate of metal uptake in the batch experiments was modeled using a pseudo-first-order equation: $d[Me]/dt = -k_{obs}[Me]$, where Me is the metal or metalloid molar concentration, k_{obs} is the rate constant, and t is time. Integration of the above equation and incorporation of Me^0 as the initial Me concentration gives:

$\ln[Me] = \ln[Me^0] - k_{obs}t$. Because the uptake rate of metals from solution was shown to depend on the availability of Fe^0 surface area, specific reaction rates were determined using $k_{sa} = k_{obs}/\rho_a$ where $\rho_a = a_s\rho_m$, a is the specific surface area of Fe^0 ($m^2\,g^{-1}$), and ρ_m is the mass concentration of Fe^0 in the batch experiment ($g\,l^{-1}$) (see Johnson et al., 1996).

In the batch experiments, pseudo-first-order kinetics can be identified over the initial 50 h of the experiments (Fig. 3). Over this time interval linear trends are revealed on plots of ln[Me] versus time. At $t > 50$ h, linear trends are evident, but slopes decease by a factor of approximately 11–35 times and data trends tend to be more scattered. These observations are likely due to changes in uptake mechanisms with time, changing reaction kinetics as equilibrium is approached, and to lower analytical precision as the limits of detection are approached at greater reaction times.

In Table 2 rate constants are presented that correspond to the initial rapid removal stage of the batch experiments. In all cases, regression analyses gave R^2 values greater than 0.92. Initial uptake rates were independent of the initial pH, yet it is acknowledged that the rate constants in Table 2 are determined for systems with variable pH. Removal rates for the metals examined in this study follow Al > Cu > As > Cd > Ni > Zn. Reaction half-lives ranged from 1.50 ± 0.09 h for Al to 8.15 ± 0.36 h for Zn (Table 2). Previous studies examining zero-valent iron–metal interactions have not presented rate constants with which to compare the results of this study. Su and Puls (2001) reported on arsenite and arsenate removal by zero-valent iron from dilute NaCl solutions. Their surface-normalized rate constant for As(V) uptake onto Peerless Iron was 0.572 ± 0.033 $ml\,h^{-1}\,m^{-2}$, which is slightly greater but in reasonable agreement with the value reported in Table 2 (0.33 ± 0.06 $ml\,h^{-1}\,m^{-2}$), especially considering the differences in solution chemistry between the different studies.

3.5. Precipitate formation

In all batch experiments, visual observations confirmed the formation through time of fine-grained, green-colored solid precipitates. Precipitates were removed from several batch tests by successive ultrasonic agitation and filtration in an anaerobic glovebox. The separated material was analyzed by X-ray powder diffraction techniques. Results of typical diffraction scans indicate that the dominant corrosion product was sulfate green rust (GR2) (Fig. 4). Green rust (GR) compounds are compositionally variable, mixed valence Fe(II)/Fe(III) layered hydroxides (Bernal et al., 1959; Hanson, 1989). Green rust structural units consist of alternating positively charged tri-octahedral metal hydroxide sheets and negatively charged interlayers of anions (Taylor, 1973). Anions present in the interlayer

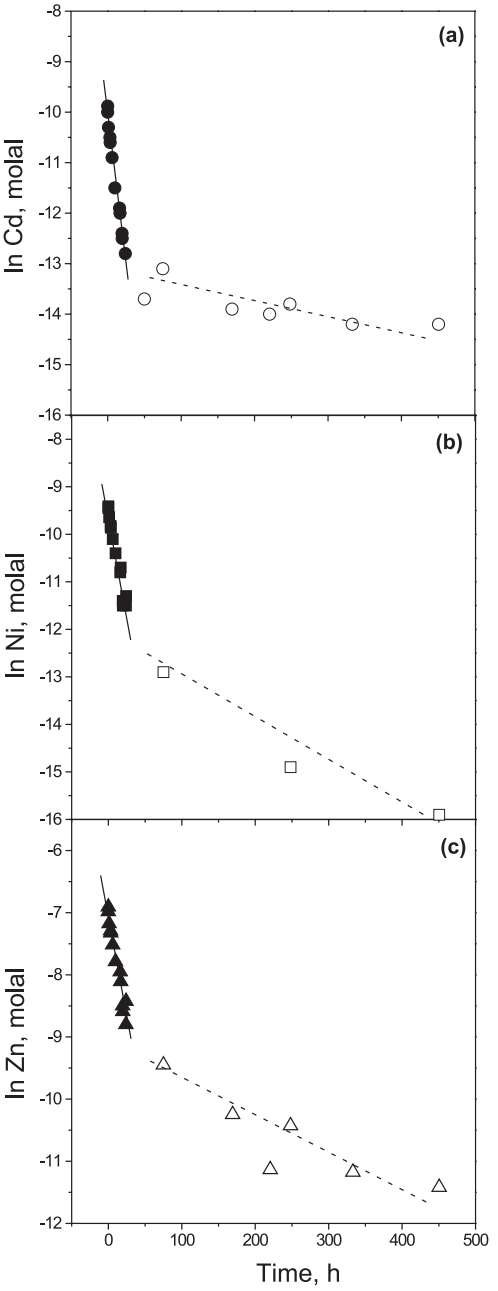

Fig. 3. Pseudo-first-order rate plots for: (a) cadmium, (b) nickel, and (c) zinc.

positions typically are Cl^-, CO_3^{2-}, or SO_4^{2-}. Two types of GR are distinguishable based upon X-ray analyses: GR1 in which the distance between hydroxide sheets is between about 0.75 and 0.80 nm (e.g., $GRCO_3^{2-}$) and GR2 in which the distance between sheets is about 1.1 nm (e.g., $GRSO_4^{2-}$). The three predominant d-spacings at 1.14, 0.58, and 0.37 confirm the formation of GR2 in the batch experiments (Fig. 4).

Table 2
Pseudo-first-order rate constants, surface area-normalized rate constants, and normalized half-lives for metal removal by Fe^0 (Peerless)

Metal	k_{obs} (h^{-1})	k_{sa} ($ml\,h^{-1}\,m^{-2}$)	$t_{1/2}$ (h)
Al	0.35 ± 0.02	0.46 ± 0.03	1.5 ± 0.1
As(V)	0.25 ± 0.05	0.33 ± 0.06	2.1 ± 0.3
Cd	0.12 ± 0.01	0.15 ± 0.01	4.6 ± 0.2
Cu	0.27 ± 0.02	0.35 ± 0.02	2.0 ± 0.1
Hg	$\geqslant 0.25$	$\geqslant 0.32$	
Ni	0.08 ± 0.01	0.11 ± 0.01	6.3 ± 0.4
Zn	0.07 ± 0.003	0.09 ± 0.004	8.2 ± 0.4

Note: $t_{1/2}$ calculated assuming a surface area loading of 1 $m^2\,ml^{-1}$.

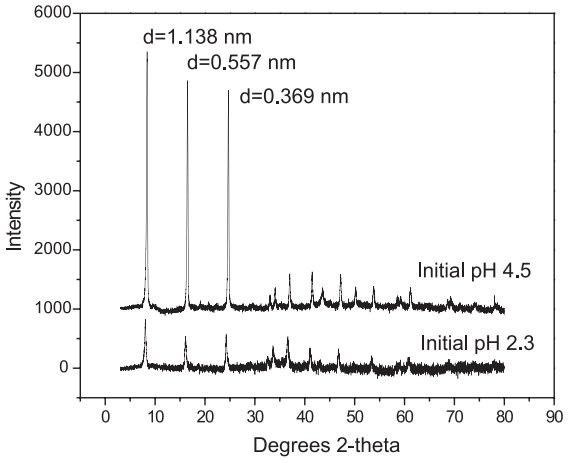

Fig. 4. X-ray diffraction patterns for precipitates formed during batch experiments.

Because sulfate was the dominant anion present in the batch experiments, the ideal composition of the precipitated GR2 is likely $Fe_6(OH)_{12}SO_4 \cdot nH_2O$. The total sulfur concentration in the material was determined to be 4.46 ± 0.04 wt.% S by sulfur coulometry, which is consistent with a n value of 4.

Solid-phase characterization and geochemical modeling studies of iron corrosion in full-scale PRBs indicate that in non-mining impacted groundwater, carbonate forms of green rust precipitate preferentially over the sulfate form in zero-valent iron systems (e.g., Wilkin et al., 2002). These observations can be understood by considering the following exchange equilibrium based upon the anhydrous GR components:

$$Fe_6(OH)_{12}SO_4 + CO_3^{2-} = Fe_6(OH)_{12}CO_3 + SO_4^{2-}$$

So that

$$K_1 = [SO_4^{2-}/CO_3^{2-}] \cdot [Fe_6(OH)_{12}CO_3/Fe_6(OH)_{12}SO_4]$$

Assuming ideal mixing relations in the solids and taking thermodynamic data from Bourrié et al. (1999) for the anhydrous carbonate and sulfate forms of green rust, we estimate $K_1 = 10^{3.1}$. The $[SO_4^{2-}/CO_3^{2-}]$ ratio in our experimental solutions was in all cases $>10^{3.7}$, consistent with the predominance of sulfate green rust over carbonate green rust in the batch experiments. Consequently, GR2 is expected to be a primary iron corrosion product as acidic, sulfate-rich and bicarbonate-poor waters interact with zero-valent iron.

Acid digestion and analysis of the GR2 suggests that it is enriched in Ni (0.05–0.21 wt.%), As (0.04–0.51 wt.%), Cu (1.3–3.0 wt.%), and Zn (0.90–1.3 wt.%). Metal uptake by GR2 via adsorption or co-precipitation processes may be important mechanisms responsible for metal removal by zero-valent iron. Refait et al. (1994) demonstrated that Ni^{2+} could partially or completely substitute for Fe^{2+} in the carbonate green rust structure. It seems reasonable that the green rust structure could accommodate other divalent ions present in octahedral coordination, including Cu^{2+} and Zn^{2+} (Cavani et al., 1991). Arsenic could possibly substitute for sulfate in the anionic interlayer. Particle morphology of the green rust material formed in the batch experiments is shown in Fig. 5. EDX analysis confirms the presence of iron, oxygen, copper, zinc, aluminum, and sulfur.

3.6. Solution saturation states

Bourrié et al. (1999) proposed the following solubility controlling equation for sulfate green rust: $\log K_{sp} = 9.43 \pm 0.4 = \log[Fe^{2+}] + 2pH - 1/3\log[e^-] + 1/6\log[SO_4^{2-}]$. In this equation, the activity of the electron can be qualitatively evaluated from the relation: $\log[e^-] = -FE_h(\alpha RT)^{-1}$ where T is temperature (K), F is the Faraday constant, and R is the molar gas constant. In Fig. 6a, the logarithm of the ion activity product (IAP)

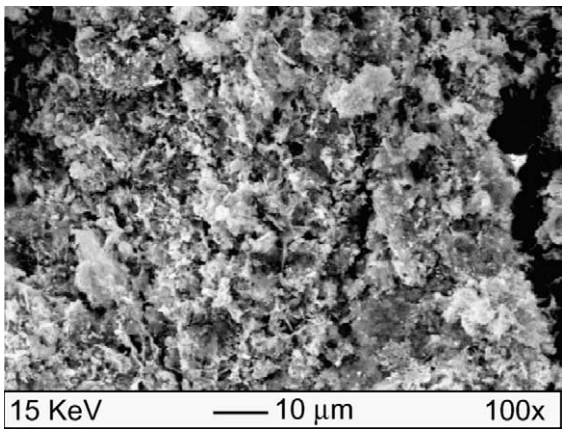

Fig. 5. Representative SEM micrograph of corrosion products formed during batch reactions with zero-valent iron.

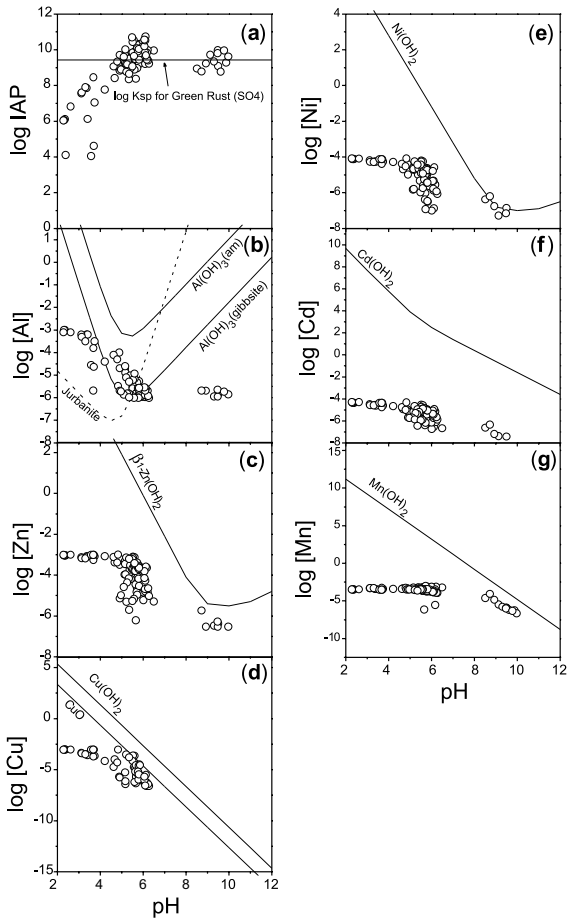

Fig. 6. Metals concentrations as a function of pH compared to solubility of sulfate green rust and metal hydroxides.

is plotted as a function of pH for sulfate green rust. At pH below about 5, the batch solutions were undersaturated with respect to sulfate green rust, i.e., $\log \mathrm{IAP} < \log K_{sp}$. Above pH 5, solution IAPs appear to cluster around the $\log K_{sp}$ value of 9.43 suggesting that the batch solutions were saturated in sulfate green rust. The relatively large amount of scatter evident in Fig. 6a is likely due to the use of E_h in the calculation of log IAP. E_h is more appropriately used as a qualitative indicator of solution redox state rather than as a thermodynamic operator (Langmuir, 1997). Nevertheless, the trends in solution chemistry and E_h are consistent with the solid-phase studies showing the formation of sulfate green rust as a primary corrosion product and control on the concentrations of iron and sulfate in solution.

The observed metals concentrations are compared to the pH-dependent solubility of the simple metal hydroxides in Fig. 6b–f. Thermodynamic constants for metal hydrolysis reactions and metal hydroxide solubility products were taken from Baes and Mesmer (1976) for Zn, Ni, Cd, and Mn, from Langmuir (1997) for Al, and from Hidmi and Edwards (1999) for Cu. Ion activity coefficients were obtained using the "B-dot" version of the extended Debye–Hückel equation. A, B, and B-dot parameters were taken from Helgeson (1969) and ion size parameters were taken from Kielland (1937). This method for determining ion activity coefficients is appropriate for solutions with ionic strengths less than about 0.5. In this study, solution ionic strengths were always less than 0.3.

Inspection of Fig. 6 shows that in all cases the batch solutions were initially highly undersaturated (pH < 4) with respect to the various metal hydroxide forms. In the case of Al (Fig. 6b), solutions appear to approach saturation with respect to gibbsite ($Al(OH)_3$) over the pH interval from about 4 to 7. At more alkaline pH from 8 to 10.5, Al is again undersaturated with respect to both amorphous $Al(OH)_3$ and gibbsite. This behavior suggests that Al may be present in a more stable form within the reactive material relative to aluminum hydroxide or that dissolution rates of aluminous materials are retarded, perhaps due to armoring by iron corrosion products. Jurbanite ($AlSO_4OH \cdot 5H_2O$) does not appear to be an important control on aluminum concentrations even at low pH where it is predicted to be the stable aluminum phase (Fig. 6b).

Potential solubility controls do not reproduce the observed concentration data for zinc, nickel, and cadmium (Fig. 6c–e, g). The rapid removal of these metals over the first several hours of reaction is not likely due to precipitation of a metal hydroxide but rather is more likely due to adsorption, although it is possible that precipitation of more complex mixed precipitates was occurring as an early reaction process. At pH > 8, zinc, nickel, and manganese may be controlled by metal hydroxide solubility and copper concentrations appear to be controlled by the solubility of CuO. Over the entire pH range studied, solution compositions were always undersaturated with respect to $Cd(OH)_2$ so that Cd removal was likely due to adsorption onto corrosion products (Fig. 6f).

The possible control of metal concentrations by surface adsorption reactions was explored by taking ferrihydrite as a model solid at solution loadings from 0.005 to 0.03 $\mathrm{g\,ml^{-1}}$ and a specific surface area of 600 $\mathrm{m^2\,g^{-1}}$ (Dzombak and Morel, 1990). Ferrihydrite is a reasonable model material that might be present as thin corrosion layers on zero-valent iron particles prior to reaction. Surface protonation constants for metal complexation were from Dzombak and Morel (1990). The adsorption of As, Cu, Cd, and Zn onto ferrihydrite could be used to explain the observed data trends (Fig. 7a). However, adsorption reactions for Hg and Ni on ferrihydrite do not reproduce the experimental results (e.g., Fig. 7b). More accurate fits of the metal concentrations might be obtained by adding other surfaces,

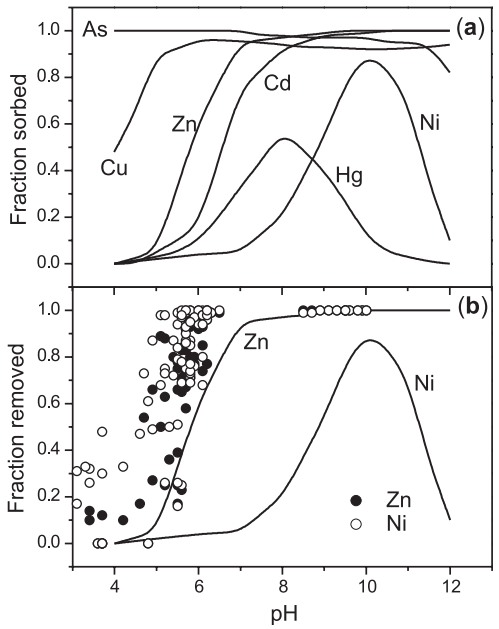

Fig. 7. Results of model calculations: (a) metal and metalloid sorption as a function of pH onto a hydrous ferric hydroxide surface (initial concentrations: As = 10 mg l^{-1}; Cu = 50 mg l^{-1}; Cd = 5 mg l^{-1}, Hg = 3 mg l^{-1}; Ni = 5 mg l^{-1}; Zn = 50 mg l^{-1}; $Fe(OH)_3$ (s) = 0.03 g ml^{-1}; (b) model results for Zn and Ni compared to observed metal removal in batch experiments.

such as green rust, however, the necessary data for this modeling are currently unavailable.

Shokes and Möller (1999) proposed that copper and cadmium are rapidly reduced and plated onto the iron surface. Combining half-cell reactions for copper reduction and iron metal oxidation we obtain:

$$Cu^{2+} + Fe^0 = Fe^{2+} + Cu^0$$

with $\log K = 26.3$. Analysis of $\log K$ values for redox reactions involving metal reduction and iron metal oxidation indicates that plating is thermodynamically favored for mercury, copper, nickel and cadmium in the order $Hg \gg Cu > Ni > Cd$. Comparing, for example, solution Fe/Cu activity ratios in the batch experiments with $10^{26.3}$ does not support an equilibrium plating process in these batch experiments. In addition, solid-phase characterization studies did not reveal the presence of elemental copper, nickel or cadmium. However, given the strong driving force for reduction of Hg^{2+} to Hg^0 when coupled to iron corrosion, the fast removal of mercury from solution (Fig. 2), and the inability of surface adsorption to completely account for mercury removal, it seems reasonable that plating represents an important mercury removal process in zero-valent iron systems. More experimental data are needed to evaluate this process.

3.7. Reversibility

Reversibility is a key issue regarding the selection of reactive materials that might be considered for use in a permeable barrier for groundwater cleanup. Temporal or spatial changes in groundwater chemistry, especially with respect to changes in pH or redox conditions, could impact the long-term performance of subsurface treatment systems by changing geochemical conditions in such a way that contaminant mobilization becomes favored over attenuation. Reversibility was explored by (i) purging batch systems after about 450 h of reaction with air, and (ii) adjusting pH from the final alkaline values attained in the batch runs to pH < 2. Reoxidation (by bubbling the batch systems with air for a 24 h time period) was ineffective in remobilizing metals previously removed by the zero-valent iron. During aeration the formation of iron oxyhydroxide was evident, but detectable levels of dissolved metals were not observed in solution. This suggests that zero-valent iron (plus oxidation products) is able to retain metals over a wide range of redox conditions and that metal uptake is largely irreversible with respect to changes in redox conditions. It should be noted that continued input of air-saturated solutions to zero-valent iron will eventually lead to cementation and significant loss of pore space (see Liang et al., 2000). Conversion of iron metal to goethite results in a volume gain 13.1 cm^3 per mole of iron reacted, which is a significant increase in volume that will likely impact porosity and permeability of reactive media placed in the subsurface. For example, 20% conversion of iron metal to goethite will result in a fractional porosity reduction of about 0.2, assuming that all iron is conserved in the solid phase.

Acid extraction tests indicated that metals were released once solution pH decreased to below 4, however, complete metal recovery was not obtained even at pH 2. Consequently, once the acid-neutralizing capacity of zero-valent is exhausted, continued acid introduction will lead to partial remobilization of metals. The theoretical acid-neutralization capacity of iron metal is 36 000 μmol H^+ g^{-1} of iron, but it is expected that the actual capacity will be less than this calculated quantity. Results from this study indicate an acid-neutralization capacity of at least 230 μmol H^+ g^{-1} of iron or greater than 0.63% of the theoretical value. Amendments of limestone, for example, to zero-valent iron media may add additional neutralizing capacity to improve remedial performance.

4. Conclusions

As pointed out by Shelp et al. (1995) and Shokes and Möller (1999), zero-valent iron is effective in rapidly neutralizing acid and promoting removal and

immobilization of dissolved heavy metals. The results of this study indicate that rapid metal removal is due to adsorption onto the iron metal surface or onto iron corrosion products initially present on the unreacted metal surface. In sulfate-rich solutions typical of AMD impacted groundwater, the sulfate form of green rust is a primary corrosion product of zero-valent iron. This finding contrasts with most previous PRB applications where bicarbonate-rich groundwaters lead to the precipitation of various carbonate precipitates including aragonite, calcite, and the carbonate form of green rust. Continued adsorption onto iron corrosion products and co-precipitation with corrosion products, or both, are likely to be secondary and slower metal uptake processes.

Other factors that will contribute to the performance of zero-valent iron in mine-impacted groundwater are the role of microorganisms and the effect of high TDS loads. The metabolic activity of sulfate-reducing bacteria in zero-valent iron systems has been well documented (e.g., Phillips et al., 2000; Roh et al., 2000; Wilkin et al., 2002). The presence of these organisms will offer additional pathways for metal removal, i.e., precipitation of insoluble metal sulfides. High TDS loads are expected to lead to higher rates of mineral precipitation and loss of pore space and permeability. The results of this study show that relatively low density calcium and magnesium carbonates, the most common authigenic precipitates in bicarbonate-dominated groundwater, are not expected in sulfate-dominated mine waste-impacted groundwater. Depending on input pH, significant accumulations of precipitates containing iron, aluminum, and manganese might be expected. Sulfate removal by zero-valent iron in abiotic systems is incomplete. Limited formation of sulfate green rust and possible precipitation of high-density metal sulfides will act to counter the effect of high solute inputs to reactive media with respect to pore infilling.

Acknowledgements

We would like to acknowledge the analytical support provided by ManTech Environmental Research Services Corporation. The US Environmental Protection agency through its Office of Research and Development funded the research described here. It has not been subjected to Agency review and therefore does not necessarily reflect the views of the agency, and no official endorsement should be inferred. Mention of trade names or commercial products does not constitute endorsement or recommendation for use.

References

Baes, C.F., Mesmer, R.E., 1976. Hydrolysis of Cations. Wiley Interscience, New York.

Barnes, I., Clarke, F.E., 1964. Geochemistry of ground water in mine drainage problems. Geological Survey Professional Paper 473-A, 6p.

Benner, S.G., Blowes, D.W., Ptacek, C.J., 1997. A full-scale porous reactive wall for prevention of acid mine drainage. Ground Water Monit. Rem. 17, 99–107.

Benner, S.G., Blowes, D.W., Gould, W.D., Herbert Jr., R.B., Ptacek, C.J., 1999. Geochemistry of a permeable reactive barrier for metals and acid mine drainage. Environ. Sci. Technol. 33, 2793–2799.

Bernal, J.D., Dasgupta, D.T., Mackay, A.L., 1959. The oxides and hydroxides of iron and their structural interrelationships. Clay Mineral. Bull. 4, 15–30.

Blowes, D.W., Ptacek, C.J., 1994. Acid-neutralization mechanisms in inactive mine tailings. In: Blowes, D.W., Jambor, J.L. (Eds.), Environmental Geochemistry of Sulfide-Mine Wastes. In: Short Course Handbook, vol. 22. Mineralogical Association of Canada, Waterloo, pp. 271–292.

Blowes, D.W., Ptacek, C.J., Benner, S.G., McRae, C.W.T., Bennet, T.A., Puls, R.W., 2000. Treatment of inorganic contaminants using permeable reactive barriers. J. Contam. Hydrol. 45, 123–137.

Bourrié, G., Trolard, F., Génin, J., Jaffrezic, A., Maître, V., Abdelmoula, M., 1999. Iron control by equilibria between hydroxy-green rusts and solutions in hydromorphic soils. Geochim. Cosmochim. Acta 63, 3417–3427.

Cantrell, K.J., Kaplan, D.I., Wietsma, T.W., 1995. Zero-valent iron for the in situ remediation of selected metals in groundwater. J. Hazard. Mater. 42, 201–212.

Cavani, F., Trifirò, F., Vaccari, A., 1991. Hydrotalcite-type anionic clays: Preparation, properties, and applications. Catal. Today 11, 173–301.

Drury, W.J., 1999. Treatment of acid mine drainage with anaerobic solid-substrate reactors. Water Environ. Res. 71, 1244–1250.

Dvorak, D.H., Hedin, R.S., Edenborn, H.M., McIntire, P.E., 1992. Treatment of metal-contaminated water using bacterial sulfate reduction: Results from pilot scale reactors. Biotechnol. Bioengin. 40, 609–616.

Dzombak, D.A., Morel, F.M.M., 1990. Surface Complexation Modeling: Hydrous Ferric Oxide. John Wiley and Sons, New York.

Gui, J., Devine, T.M., 1994. The influence of sulfate ions on the surface enhanced Raman spectra of passive films formed on iron. Corros. Sci. 36, 441–462.

Hanson, H.C.B., 1989. Composition, stabilization, and light absorption of Fe(II)Fe(III) hydroxy carbonate (green rust). Clay Mineral. 24, 663–669.

Helgeson, H.C., 1969. Thermodynamics of hydrothermal systems at elevated temperatures and pressures. Am. J. Sci. 63, 622–635.

Hidmi, L., Edwards, M., 1999. Role of temperature and pH in $Cu(OH)_2$ solubility. Environ. Sci. Technol. 33, 2607–2610.

Johnson, T.L., Scherer, M.M., Tratnyek, P., 1996. Kinetics of halogenated organic compound degradation by iron metal. Environ. Sci. Technol. 30, 2634–2640.

Kielland, J., 1937. Individual activity coefficients of ions in solutions. J. Am. Chem. Soc. 59, 1675–1678.

Kleinmann, R.L.P., 1989. Acid mine drainage in the United States controlling the impact on streams and rivers. In: 4th

World Congress on the Conservation of the Built and Natural Environments, University of Toronto, pp. 1–10.

Lackovic, J.A., Nikolaidis, N.P., Dobbs, G.M., 2000. Inorganic arsenic removal by zero-valent iron. Environ. Eng. Sci. 17, 29–39.

Langmuir, D.E., 1997. Aqueous Environmental Geochemistry. Prentice Hall, Upper Saddle River, NJ.

Liang, L., Korte, N., Gu, B., Puls, R., Reeter, C., 2000. Geochemical and microbial reactions affecting the long-term performance of in situ 'iron barriers'. Adv. Environ. Res. 4, 273–286.

Lowson, R.T., 1982. Aqueous oxidation of pyrite by molecular oxygen. Chem. Rev. 82, 461–497.

Morrison, S.J., Metzler, D.R., Dwyer, B.P., 2002. Removal of As, Mn, Mo, Se, U, V, and Zn from groundwater by zero-valent iron in a passive treatment cell: reaction progress modeling. J. Contam. Hydrol. 56, 99–116.

Nordstrom, D.K., Jenne, E.A., and Averett, R.C., 1977. Heavy metal discharges into Shasta Lake and Keswick Reservoir on the Upper Sacramento River, California—A reconnaissance during low flow. United States Geological Survey Open-File Report 76-49, 25p.

Phillips, D.H., Gu, B., Watson, D.B., Roh, Y., Liang, L., Lee, S.Y., 2000. Performance evaluation of a zerovalent iron reactive barrier: Mineralogic characterization. Environ. Sci. Technol. 34, 4169–4176.

Puls, R.W., Blowes, D.W, Gillham, R.W., 1999. Long-term performance monitoring for a permeable reactive barrier at the US Coast Guard Support Center, Elizabeth City, North Carolina. J. Hazard. Mater. 68, 109–124.

Refait, P., Drissi, H., Marie, Y., Génin, J., 1994. The substitution of Fe^{2+} ions in green rust one compounds. Hyperfine Interact. 90, 389–394.

Roh, Y., Lee, S.Y., Elless, M.P., 2000. Characterization of corrosion products in the permeable reactive barriers. Environ. Geol. 40, 184–194.

Shelp, G.S., Chesworth, W., Spiers, G., 1995. The ameloriation of acid mine drainage by an in situ electrochemical method—I. Employing scrap iron as the sacrificial anode. Appl. Geochem. 10, 705–713.

Shokes, T.E., Möller, G., 1999. Removal of dissolved heavy metals from acid rock drainage using iron metal. Environ. Sci. Technol. 33, 282–287.

Steed, V.S., Suidan, M.T., Gupta, M., Miyahara, T., Acheson, C.M., Sayles, G.D., 2000. Development of a sulfate-reducing biological process to remove heavy metals from acid mine drainage. Water Environ. Res. 72, 530–535.

Su, C., Puls, R.W., 2001. Arsenate and arsenite removal by zerovalent iron: kinetics, redox transformation, and implications for in situ groundwater remediation. Environ. Sci. Technol. 35, 1487–1492.

Taylor, R.M., 1973. Crystal structures of some double hydroxide minerals. Mineral. Mag. 39, 377–389.

Waybrant, K.R., Blowes, D.J., Ptacek, C.J., 1998. Selection of reactive mixtures for use in permeable reactive walls for treatment of mine drainage. Environ. Sci. Technol. 32, 1972–1979.

Waybrant, K.R., Ptacek, C.J., Blowes, D.W., 2002. Treatment of mine drainage using permeable reactive barriers: Column experiments. Environ. Sci. Technol. 36, 1349–1356.

Wilkin, R.T., Puls, R.W., Sewell, G.W., 2002. Long-term performance of Permeable Reactive Barriers: An evaluation at two sites. US EPA Environmental Research Brief, EPA/600/S-02/001, 18 p.

Williamson, M.A., Rimstidt, J.D., 1994. The kinetics and electrochemical rate-determining step of aqueous pyrite oxidation. Geochim. Cosmochim. Acta 58, 5443–5454.